

Excitation of superpositions of resonances by two time-delayed ultrafast pulses: Multistate semianalytic formalism and application to inner-hole states of carbon at the K absorption edge

Yannis Komninos,^{*} Theodoros Mercouris,[†] and Cleanthes A. Nicolaides[‡]
*Theoretical and Physical Chemistry Institute, National Hellenic Research Foundation,
 48 Vasileos Constantinou Avenue, Athens, 11635, Greece*

 (Received 29 January 2020; accepted 15 April 2020; published 11 May 2020)

We construct and solve semianalytically a pump-probe problem which is defined by an excitation-coupling scheme that engages *superpositions* of resonance states. The scheme is $|0\rangle \xrightarrow[\text{attosec pulse } \omega_1]{\text{weak}}$ (superposition of resonances) $\xleftrightarrow[\text{femtosec pulse } \omega_2]{\text{moderately strong}}$ (superposition of resonances) where $|0\rangle$ is a discrete state. The resonance wave functions are treated rigorously as stationary states in the continuous spectrum. They are energy-normalized and are expressed as linear combinations of localized and scattering components, using the formalism of Fano. The attosecond and femtosecond pulses have central frequencies ω_1 and ω_2 , with $\omega_1 \gg \omega_2$. They are applied with positive (the short XUV pulse peaks *after* the second pulse) or negative (the short XUV pulse peaks *before* the second pulse) time delay, t_D . The theory is time-dependent and involves many-electron wave functions and matrix elements. Its computational implementation is extremely economic. The application which is reported here treats the excitation of a core-excited superposition of valence-Rydberg autoionizing states of carbon near the K -absorption edge by a weak 100 as Gaussian pulse, and their coupling to a higher-lying core-excited autoionizing Rydberg state by an 80 fs Gaussian pulse of intensities of order 10^{12} W/cm². State-specific N -electron correlated wave functions are used. A number of concrete findings are obtained, demonstrating a variety of channel-dependent photoelectron spectra as functions of the pulse parameters and of the time delay, t_D .

DOI: [10.1103/PhysRevA.101.053420](https://doi.org/10.1103/PhysRevA.101.053420)

I. INTRODUCTION

A. Resonance-state superpositions in time-resolved attosecond spectroscopy

In the challenging new field of the study of electron dynamics that is time-resolved on ultrafast timescales, from a few femtoseconds (fs) down to a few attoseconds (as), it is possible to explore new types of phenomena and to obtain quantitatively physically relevant information via the application of novel experiments and theory. The initial fundamental ideas and methods were first tested on spectroscopic aspects of atomic systems, where the scrutiny of the results is facilitated by the fact that the information can be analyzed in terms of known or calculable energy states and processes. For certain representative reviews on the progress of attosecond physics and for a gleaning of original experimental and theoretical articles on time-resolved electron dynamics in atoms, the reader is referred to Refs. [1–15] and their references.

If the spectroscopic information of interest is to be obtained and understood in terms of solutions of many-electron problems involving real atomic states, rather than in terms of the often used, but hardly realistic, simple one-electron models, two fundamental issues must be dealt with: One is

the construction of the formalism for the description and calculation of time-dependent quantities with physical relevance, and the other has to do with the requirement of calculating the time-dependent solution of *many-electron* time-dependent Schrödinger equation (METDSE) the appropriate for each problem in terms of methods that can take into account those effects of electronic structures, electron correlations, and open channels, which are expected to play the dominant role in the physics of interest, as a function of the pulse parameters.

Characteristic early examples of experimental-theoretical successful results in this direction of research are the measurements and the theoretical results from many-electron calculations which revealed a difference on the order of 10 as in the photoemission of electrons initially occupying the $2s$ and $2p$ (sub)shells in neon [7,9,10,13] and the quantitative prediction and experimental observation of the time-resolved build-up of the doubly excited $2s2p\ ^1P^o$ resonance state of helium, whose completion takes about 180 fs [11,12].

The year 2001 saw the first report of the generation in the laboratory of single attosecond pulses [4] and of trains of attosecond pulses [5]. The announcement of those experimental breakthroughs inevitably gave birth to a crucial question: What type of systems and of novel phenomena could be investigated spectroscopically and reliably on attosecond timescales?

In response to this rhetorical question, in 2002 [6] and in subsequent publications, we presented our theory and showed quantitatively how the preparation of the transient

^{*}ykomn@eie.gr

[†]thmerc@eie.gr

[‡]caan@eie.gr

superpositions of doubly excited and of inner-hole autoionizing states, both types belonging to the continuous electronic spectrum, can create conditions for the study of multielectron dynamics of excitation and decay that occur on such ultrashort scales.

The superpositions of electronic resonances in Ref. [6] were initiated by the simultaneous application of two femtosecond pulses of different frequencies. On the other hand, the normal way for achieving preparation of superposition of states is the application of a single pulse that is sufficiently broad in energy so as to excite more than one state that are relatively in proximity. Traditionally, such preparations have involved discrete states, using pulses which are not spectrally very broad (e.g., excitation of superpositions of Rydberg levels).

In the context of experimental attosecond physics, an example of the preparation of superposition of electronic states and of its use for probing aspects of electron dynamics is the experiment by Goulielmakis *et al.* [8], where the method of attosecond transient absorption spectroscopy was demonstrated. Specifically, the scheme was based on the preparation of a superposition in the Kr ion of the $J = 3/2$ and $1/2$ discrete levels by quick ionization of Kr from the $4p$ shell by a single pulse which covers energetically both levels, and the probing of this superposition by an attosecond pulse around 150 as involving the $3d \rightarrow 4p$ excitation [8].

In this paper, we present a formalism and its computational implementation on another type of time-resolved pump-probe scheme, where the initial excitation reaches directly the continuous spectrum and excites a superposition of *resonance states*, which is coupled by a second pulse to another superposition of *resonance states*. The two-pulse, two-color, many-electron problem is time-dependent in terms of both the excitation amplitudes and the mixing coefficients of the resonances and *involves directly the continuous spectrum*.

As is well known, the quantum mechanics of resonance states is significantly more complex than that describing the discrete states. Since the late 1920s, it has been recognized that their wave functions have an energy dependence and consist of two components: one which is localized, and one which is unbound, with scattering boundary conditions in the asymptotic region. For N -electron systems, it is crucial that the localized component is represented by a reliably calculated square-integrable N -electron wave packet including the dominant electron correlations that contribute to its localization [16] and subsequent publications.

The problem has to do with a scheme—see A below—whereby time-dependent probabilities of emission of photoelectrons into different open channels can be computed as a function of pulse duration, of frequency on- and off-exact

resonance, and of intensity and of the *time delay*, t_D , in the application of the two pulses. The distinction of different channels is achievable via the measurement of the energies and the angular distributions of the photoelectrons.

The theory and methodology which are discussed in the following sections constitute a very economic, yet reliable, approach for dealing computationally with such problems. Central to this approach is the expansion in terms of eigenfunctions, for each angular momentum and parity subspace which are coupled by the presence of electromagnetic fields. This feature provides serious advantages, since, when the continuous spectrum is directly involved in any phenomenon whose understanding requires the solution from first principles of the METDSE, the theoretical task becomes computationally overwhelming, even if the formalism is in place. This fact has been emphasized in a series of papers where the METDSE pertinent to each problem has been solved numerically using the *state-specific expansion approach* (SSEA). The SSEA solution determines how the time-dependent nonstationary state evolves over the stationary states of the discrete and of the continuous spectrum. However, in order for convergence to be achieved, one has to construct and solve many thousands of coupled integrodifferential equations containing, in addition to *bound-bound* and *bound-free* dipole matrix elements, the huge number of *free-free* matrix elements (on- and off-resonance), with energy-normalized, numerically calculated scattering functions [6,12,17]. The *free-free* matrix elements have singularities on the energy axis, whose accurate calculation has required special mathematical and numerical treatment [17].

The present problem is solved in terms of a semianalytic *multistate* formalism, whose implementation is carried out using many-electron discrete and resonance wave functions. We solve a time-dependent n -level (TDnL) system with $n = N_1 + N_2 + 1$, where the N_1 resonance levels are contained in the first ionization channel and the N_2 resonance levels in the second one. This is achieved mainly in terms of analytic formalism. Numerical procedures are followed for the diagonalization of the resulting matrices. The formalism contains basic elements of the recently published theory for the solution of the time-dependent three-level (TD3L) system of *discrete-resonance-resonance* excitation and coupling scheme [18], which yields analytic expressions for photoelectron emission probabilities, $P_i(E, t)$, $i = 1, 2$, in the energy region of the two resonance states. The extension to the general case of excitation and field-coupling of *superposition* of resonance states is necessary when the pulses are spectrally broad, as is normally the case with attosecond pulses.

The physical scheme of interest involves the excitation and coupling of superpositions of resonance states by two ultrafast pulses:

$$|0\rangle \xrightarrow[\text{attosec pulse } \omega_1]{\text{weak}} (\text{superposition of resonances}) \xleftarrow[\text{femtosec pulse } \omega_2]{\text{moderately strong}} (\text{superposition of resonances}) \quad (\text{A})$$

where $|0\rangle$ is a discrete state. The resonance wave functions are treated rigorously. They are energy-normalized (Dirac normalization) and are expressed as linear combinations of localized and scattering components. The attosecond and

femtosecond pulses have central frequencies ω_1 and ω_2 , with $\omega_1 \gg \omega_2$. They are applied with positive (the short XUV pulse peaks *after* the second pulse) or negative (the short XUV pulse peaks *before* the second pulse) time delay, t_D .

The choice of the scheme A is related to a variety of possible many-electron systems, when a high-energy, spectrally broad attosecond pulse is used for the first step of excitation into the continuous spectrum where electronic resonance states exist. However, the formalism and the overall approach are not restricted only to such situations.

The structure of the theory is such that it is not limited to two-electron states. It is applicable to DESs as well as to *inner-hole excited* states of many-electron atoms and molecules lying deep inside the continuum. Although the basic features of the formal theory for these two classes of states are essentially the same (they are unstable states in the continuum), when it comes to the calculation of their wave functions and energies, and of phenomena which depend on transition matrix elements, the treatments have certain critical differences that depend on electronic structures, on the nature of electron correlations, on spectra, on the degree of contribution of each open channel, etc. This holds for non-relativistic as well as for relativistic Hamiltonians. In practice, the calculation employs N -electron transition matrix elements, where *nonorthonormality* (NON) between the state-specific basis functions is taken into account explicitly.

As a prototypical application, we constructed and solved a many-electron problem involving the photoexcitation or ionization of the $1s$ electron of carbon. This is the K -shell attosecond-pulse excitation of the C $1s^2 2s^2 2p^2 \ ^3P$ ground state to a superposition of two autoionizing states of carbon of $^3S^o$ symmetry, one valence and one Rydberg state, which are coupled by a second ultrashort pulse, with time delay t_D , to a higher-lying autoionizing state (Rydberg) of 3P symmetry. Both pulses have Gaussian temporal shapes. The half width at half maximum of the attosecond pulse is assumed to be 100 as.

B. Attosecond-resolved processes involving two-color-excited Auger states: Application to the carbon K -absorption edge

The excitation of inner-hole states normally requires photon energies that are much larger than those needed for double excitations of valence electrons. This means that, if the theory corresponding to scheme A is to be applied to such cases, the frequency ω_1 of the attosecond pulse responsible for the creation of the inner-shell hole must be relatively large. Fortunately, the continuing progress in attosecond technology now allows the approach of regimes where well-controlled attosecond pulses with high energy can be produced [19].

For example, Li *et al.* [20] reported the generation and use of soft x-ray pulses having the duration of only 53 as. They “demonstrated single pulse streaking reaching the carbon K -absorption edge (284 eV) by utilizing intense two-cycle driving pulses near $1.8\text{-}\mu\text{m}$ center wavelength” (abstract of Ref. [20]). In their discussion, they pointed to the experiment on light-induced chemical reactions by Pertot *et al.* [21] who developed and applied a table-top arrangement of time-resolved x-ray absorption spectroscopy with temporal resolution limited to 40 fs and argued that “The x-ray source demonstrated in this work makes it practical to observe [with attosecond resolution] charge migration by exploiting transition from the carbon core level to the unoccupied valence orbitals at the carbon K -edge.” Their application to CO_2 produced an absorption spectrum with a main peak at 290.77 eV

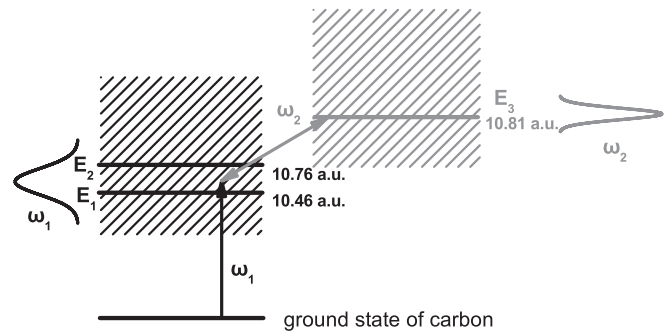


FIG. 1. The carbon excitation scheme interacting with a soft x-ray (ω_1) pulse plus a near-infrared one (ω_2) of Gaussian temporal shapes. As shown above, the carbon ground state is connected, via the (ω_1) pulse, with the resonance states E_1 ($1s2s^2 2p^3 \ ^3S^o$) and E_2 ($1s2s^2 2p^2 3p \ ^3S^o$), contained in the $1s^2 2s^2 2p^2 \epsilon p \ ^3S^o$ zero-order channel. With an ultrashort positive or negative *time delay*, t_D , the (ω_2) pulse connects them to the state E_3 [$1s2s^2 2p^2 (^4P) 3d \ ^3P$], which is embedded in the $1s^2 2s^2 2p \epsilon p \ ^3P$ zero-order channel. The energies above the ground state are given on the graph. The results given in this paper were obtained for the case of resonant two-photon coupling of the carbon ground state with the state E_3 [$1s2s^2 2p^2 (^4P) 3d \ ^3P$], which is equivalent to the condition $\omega_1 + \omega_2 = E_3$. The calculations whose results are reported here were obtained for pulse durations 100 as for the (ω_1) pulse and 80 fs for the (ω_2) one. The black and gray curves surrounding the discrete levels represent “realistically” the energy profiles of the Gaussian pulses, with central frequencies ω_1 and ω_2 .

and a satellite peak at 292.74 eV. Using the data and the analysis reported in 1979 by Tronc *et al.* [22], they assigned these peaks to excitations from the carbon $1s$ orbital to the unoccupied molecular orbital $2\pi_u^*$ (290.77 eV) and to the $3s$ Rydberg orbital (292.74 eV).

It should be noted that Li *et al.* [20] give the energy 284 eV for the K -absorption edge. This value, which corresponds to carbon in a chemical environment, is shifted considerably from the accurate, term-dependent free-atom value, known since the 1970s, which is about 296 eV [23,24]. For the many-electron approach to the advanced calculation of state-specific wave functions and of one-electron binding and Auger energies, and of widths and fluorescence yields of inner-shell states in atomic, metallic, and chemisorbed phases, the reader should consult Refs. [25–27] and related work.

The demonstration herein of the time-dependent theory involves the $1s$ -shell excitation of the C $1s^2 2s^2 2p^2 \ ^3P$ ground state to autoionizing states labeled by $1s$ -hole configurations whose outer subshells, the valence $2p$ and the Rydberg $3p$ and $3d$, are initially either incompletely occupied (in the $n = 2$ shell) or unoccupied (in the $n = 3$ shell). These orbitals are engaged in the bonding of carbon inside chemical compounds, contributing to their properties in different ways. For example, even though the $3d$ spin orbitals are not occupied in the ground state configuration of carbon, they can play an important role as virtual orbitals in calculations that pursue the accurate description of wave functions by accounting for electron correlation.

Figure 1 displays the excitation-coupling scheme for this study. The main goal was to determine the dominant features

of the photoelectron emission probability density for the resonance states in both the open channels, as a function of t_D in the order of a few femtoseconds, for various realistic values of the intensity and duration of the laser (second) pulse. In addition, the study examined the degree of sensitivity of the results to small detunings of the central frequencies. The quantitative implementation of the formalism is done in terms of N -electron wave functions with selected components of electron correlation, for which the theoretical justification and methods of calculation have been reported in our earlier publications since the 1970s; e.g., see Refs. [16,23] and the book [25].

II. PHOTOELECTRON EMISSION PROBABILITIES IN THE TD n L SYSTEM WITH TWO ULTRASHORT PULSES AND RESONANCE-RESONANCE COUPLING

The mathematical development which follows is divided into six subsections, A–F. In subsection A, the problem is formulated in terms of a time-dependent superposition that includes the localized and the asymptotically scattering *components* of the two states. The sought after amplitude of photoelectron emission probability for each channel, $A_{iE}(t)$, $i = 1, 2$, is defined in terms of the time-dependent mixing coefficients, which satisfy a system of integrodifferential equations. Subsection B presents certain physically important functions of transition matrix elements entering the calculation and the justifiable approximations which are made in order to render the system of equations solvable analytically. In subsection C, a simple transformation of the mixing coefficients allows the energy integrals to be evaluated by contour integration, and the system of integrodifferential equations is transformed into a system of ordinary differential ones. In subsection D, the latter system is solved semianalytically, assuming a rectangular temporal shape for the second pulse, while the case where this pulse has an arbitrary shape is solved by fitting it to a sum of rectangular pulses. The formal results are presented in subsection E. Finally, in subsection F an extension is made that allows many angular momenta for each parity to be included in the calculation.

A. Formal expression for the photoelectron emission probability

We consider the case where there are two open channels in which photoelectrons can be emitted. The resonance states are embedded in them. The first open channel is reached by ω_1 [the first (attosecond) pulse] and the second by ω_2 [the second (laser) pulse].

The time-dependent wave function of the system is expanded in terms of the eigenstates as ($\hbar = 1$)

$$|\Psi(t)\rangle = |\Psi_g\rangle e^{-iE_g t} c_g(t) + \sum_{i=1}^2 \int dE |\Psi_{iE}\rangle e^{-iEt} c_{iE}(t), \quad (1)$$

where Ψ_g is the ground state (or initial discrete state) of angular momentum L , $i = 1$ denotes an L or $L \pm 1$ state of the continuous spectrum, and $i = 2$ denotes an L , $L \pm 1$, or $L \pm 2$ state of the continuous spectrum. These are acting as ionization channels and have opposite parities. The electronic

Hamiltonian is thus diagonal in the continuous part of the spectrum for each angular momentum and parity.

In the subsequent development of the formalism, we shall take into account one angular momentum of the first parity and one of the second, as indicated in Eq. (1), in order to keep the treatment as simple as possible. In a final subsection (F) we shall sketch the straightforward extension of the formalism that is required in the general case of many angular momenta for each parity.

We follow Fano's formalism [28] in order to represent the stationary superposition of localized and scattering components, for each total angular momentum, of the resonance wave functions on the real energy axis. The localized components are denoted by ϕ_n and the scattering ones by $|u_{iE}\rangle$.

Let N_1 and N_2 be the number of the localized parts contained in each ionization channel, the total number being $N = N_1 + N_2$. In order to avoid double indices in numbering them, we adopt the following convention: The index n runs from 1 to N , where the values $n \leq N_1$ belong to the group of the localized parts of the first channel while those with $N_1 < n \leq N$ belong to the group of the localized parts of the second one.

Generalizing his result of a single localized part to that holding for a number of them, Fano [28] derived the expression

$$|\Psi_{iE}\rangle = \cos \Delta_i(E) \left[\sum_n \left(|\phi_n\rangle + P \int dE' |u_{iE'}\rangle \frac{1}{E - E'} V_{iE'n} \right) \times \tan \Delta_{in}(E) / \pi V_{niE} + |u_{iE}\rangle \right]. \quad (2)$$

The symbol P stands for principal-value integration and $V_{niE} = \langle \phi_n | H_{\text{atom}} | u_{iE} \rangle$ [see Eq. (65) of Ref. [28]]. In Fano's notation,

$$\tan \Delta_i(E) = \sum_n \tan \Delta_{in}(E), \quad (3a)$$

$$\tan \Delta_{in}(E) = \frac{\pi |V_{iEn}|^2}{E - E_n}, \quad (3b)$$

and

$$E_n = \langle \phi_n | H_{\text{atom}} | \phi_n \rangle + P \int dE' V_{niE'} \frac{1}{E - E'} V_{iE'n}. \quad (3c)$$

For reasons of simplicity, terms $P \int dE' V_{miE'} \frac{1}{E - E'} V_{iE'n}$ for $m \neq n$, have been neglected. In other words, we take into account the energy shift due to the interaction of the localized components with the continuum, but we neglect the second-order effect of their recoupling due to this interaction.

Note that the function $\cos \Delta_i(E)$ is zero at the energies E_n . Again following Fano, we put

$$\alpha_n(E) \equiv \cos \Delta_i(E) \tan \Delta_{in}(E) / \pi V_{niE}. \quad (4)$$

Then

$$|\Psi_{iE}\rangle = \sum_n \alpha_n(E) \left[|\phi_n\rangle + P \int dE' |u_{iE'}\rangle \frac{1}{E - E'} V_{iE'n} + |u_{iE}\rangle \frac{E - E_n}{V_{iEn}} \right]. \quad (5)$$

Thus, we have brought the total wave function to a form which is a sum of expressions that correspond to the case of a single localized component [18].

We now consider the normal case of *isolated resonances*, i.e., the case where $|E_n - E_m| \gg \frac{1}{2}(\Gamma_{in} + \Gamma_{im})$, where $\Gamma_n = \pi V_{iE_n}^2$ are the half-widths. Then for $E \approx E_n$ one obtains $\tan \Delta_i(E) \approx \tan \Delta_{in}(E)$, and, therefore,

$$\alpha_n(E) \approx \frac{V_{iE_n}}{\sqrt{(E - E_n)^2 + \Gamma_n^2}}. \quad (6)$$

The function $\alpha_n^2(E)$ has poles $z_n = E_n \pm i\Gamma_n$ above and below the real axis. They play a crucial role in the development of the present formalism [18].

The quantity of interest is the probability $P_i(E, t) \equiv |A_{iE}(t)|^2$ for $i = 1, 2$, to observe a photoelectron in one of the ionization channels with a certain angular momentum and parity. $A_{iE}(t)$ is defined below in Eq. (7). In order for it to be accurate for times when the autoionizing states have not been depleted, we subtract the survival amplitude from the total one:

$$A_{iE} = \langle \Psi_{iE} | \Psi(t) \rangle - \sum_n \alpha_n(E) \langle \phi_n | \Psi(t) \rangle. \quad (7)$$

$\Psi(t)$ satisfies the METDSE,

$$i \frac{\partial}{\partial t} \Psi(t) = \left[\mathbf{H}_{\text{atom}} + \sum_{j=1}^2 \mathbf{V}_{(j)}(\omega_j, t) \right] \Psi(t), \quad (8a)$$

where

$$\mathbf{V}_{(j)}(\omega_j, t) = z F_j g_j(t) \sin(\omega_j t - \varphi_j) \quad (8b)$$

represents the perturbation by two (ultra)short laser pulses with frequencies ω_i and envelopes $g_i(t)$. The pulses are assumed to be linearly polarized, acting with a time delay, t_D .

For the symmetries of the problem, the only nonzero dipole matrix elements are

$$D_{g,1E} = \langle \Psi_g | z | \Psi_{1E} \rangle \quad \text{and} \quad D_{1E,2\bar{E}} = \langle \Psi_{1E} | z | \Psi_{2\bar{E}} \rangle. \quad (9)$$

B. Spectral-asymmetry functions: The emergence of Fano-type complex generalized quantities (parameters)

Substituting the wave function (5) into the matrix elements (9), one has

$$D_{1E,g} = \sum_{n=1}^{N_1} \alpha_n(E) b_{nE}, \quad (10a)$$

where

$$b_{nE} \equiv d_{ng}(E) + \frac{E - E_n}{V_{n1E}} d_{1Eg}. \quad (10b)$$

Also,

$$D_{1E,2\bar{E}} \approx \sum_{n=1}^{N_1} \alpha_n(E) \sum_{m=N_1+1}^N \alpha_m(\bar{E}) b_{nE,m\bar{E}}, \quad (11a)$$

where

$$b_{nE,m\bar{E}} \equiv d_{nm}(E, \bar{E}) + \frac{E - E_n}{V_{n1E}} d_{1Em} + \frac{\bar{E} - E_m}{V_{m2\bar{E}}} d_{2En}. \quad (11b)$$

Here we have ignored the contribution of the extremely small dipole matrix elements $d_{1E,2E'} = \langle u_{1E} | z | u_{2E'} \rangle$ involving the unperturbed continua. The matrix elements $d_{ng}(E)$ and $d_{nm}(E, \bar{E})$ depend on the energy because they include the contributions from the integral of the second term in Eq. (2).

The above expressions define the quantities b_{nE} and $b_{mE,n\bar{E}}$, which we have named the *spectral-asymmetry functions* [18]. Of special interest are their values at the complex poles $z_n = E_n - i\Gamma_n$:

$$b_{nz_n} = d_{ng} - i\pi V_{n1z_n} d_{1z_ng} \quad (11c)$$

and

$$b_{nz_n,mz_m} \equiv d_{nm} - i\pi (V_{n1z_n} d_{1z_nm} + V_{m2z_m} d_{2z_mn}) \quad (11d)$$

which result as a consequence of contour integration employed in the calculation of the energy integrals of the continuous spectrum.

There are N_1 Fano discrete-resonance transition asymmetry parameters, $q_n = d_{ng}/\pi V_{n1E_n} d_{1E_n g}$, and $N_1 N_2$ *generalized asymmetry parameters* involving resonance-resonance transitions, which we have named *Q parameters*:

$$Q_{mn} = d_{mn}/(\pi V_{m1E_m} d_{1E_m n} + \pi V_{n2E_n} d_{2E_n m}). \quad (12)$$

Each Q_{mn} is associated with two branching ratios, $\gamma_{mn}^{(i)} = V_{miE} d_{iE_n}/(V_{m1E} d_{1E_n} + V_{n2E} d_{2E_m})$, $i = 1, 2$, so that $\gamma_{mn}^{(1)} + \gamma_{mn}^{(2)} = 1$. The significance of the Q parameter for the physics of resonance-resonance dipole transitions is discussed in Ref. [18].

C. The system of differential equations

The time-dependent coefficients obey the following system of equations:

$$ie^{-iE_g t} \dot{c}_g = F_1 g_1(t) \sin(\omega_1 t - \varphi_1) \int dE' D_{g,1E'} e^{-iE't} c_{1E'}, \quad (13a)$$

$$ie^{-iEt} \dot{c}_{1E} = F_1 g_1(t) \sin(\omega_1 t - \varphi_1) D_{1E,g} e^{-iE_g t} c_g + F_2 g_2(t) \sin(\omega_2 t - \varphi_2) \int dE' D_{1E,2E'} e^{-iE't} c_{2E'}, \quad (13b)$$

$$ie^{-i\bar{E}t} \dot{c}_{2\bar{E}} = F_2 g_2(t) \sin(\omega_2 t - \varphi_2) \int dE' D_{2\bar{E},1E'} e^{-iE't} c_{1E'}. \quad (13c)$$

Using the previous definitions (11), Eqs. (13) are transformed into

$$\dot{c}_g = -iF_1 e^{iE_g t} g_1(t) \sin(\omega_1 t - \varphi_1) \times \int dE' \sum_{n=1}^{N_1} \alpha_n(E') b_{nE'} e^{-iE't} c_{1E'}, \quad (14a)$$

$$\begin{aligned} \dot{c}_{1E} = & -iF_1 e^{-i(E_g - E)t} g_1(t) \sin(\omega_1 t - \varphi_1) \sum_{n=1}^{N_1} \alpha_n(E) b_{nE} c_g \\ & - iF_2 e^{iEt} g_2(t) \sin(\omega_2 t - \varphi_2) \sum_{n=1}^{N_1} \alpha_n(E) \int dE' \\ & \times \sum_{m=N_1+1}^N b_{nE, mE'} \alpha_m(E') e^{-iE't} c_{2E'}, \end{aligned} \quad (14b)$$

$$\begin{aligned} \dot{c}_{2\bar{E}} = & -iF_2 e^{i\bar{E}t} g_2(t) \sin(\omega_2 t - \varphi_2) \sum_{m=N_1+1}^N \alpha_m(\bar{E}) \\ & \times \int dE' \sum_{n=1}^{N_1} b_{m\bar{E}, nE'} \alpha_n(E') e^{-iE't} c_{1E'}. \end{aligned} \quad (14c)$$

In terms of the coefficients, Eq. (7) becomes

$$A_{iE} = e^{-iEt} c_{iE}(t) - \sum_n \alpha_n(E) \int dE' \alpha_n(E') e^{-iE't} c_{iE'}(t), \quad (7')$$

where the sum is over the localized components of the i th channel.

From inspection of Eqs. (14), it follows that the coefficients $c_{iE}(t)$ are proportional to the sum of the quantities $\alpha_n(E)$. Accordingly, we transform into the more convenient variables C_{mE} ,

$$c_{1E} = \sum_{n=1}^{N_1} \alpha_n(E) C_{nE}, \quad c_{2E} = \sum_{n=N_1+1}^N \alpha_n(E) C_{nE}, \quad (14d)$$

which satisfy the equations

$$\dot{c}_g = -iF_1 e^{iE_g t} g_1(t) \sin(\omega_1 t - \varphi_1) \int dE' \sum_{n=1}^{N_1} b_{nE'} \alpha_n(E') e^{-iE't} \sum_{k=1}^{N_1} \alpha_k(E') C_{kE'}, \quad (15a)$$

$$\begin{aligned} \sum_{n=1}^{N_1} \alpha_n(E) \dot{C}_{nE} = & -iF_1 e^{-i(E_g - E)t} g_1(t) \sin(\omega_1 t - \varphi_1) \sum_{n=1}^{N_1} \alpha_n(E) b_{nE} c_g(t) - iF_2 e^{iEt} g_2(t) \sin(\omega_2 t - \varphi_2) \sum_{n=1}^{N_1} \alpha_n(E) \int dE' \\ & \times \sum_{m=N_1+1}^N b_{nE, kE'} \alpha_k(E') e^{-iE't} \sum_{m=N_1+1}^N \alpha_m(E') C_{mE'}, \end{aligned} \quad (15b)$$

$$\sum_{m=N_1+1}^N \alpha_m(\bar{E}) \dot{C}_{m\bar{E}} = -iF_2 e^{i\bar{E}t} g_2(t) \sin(\omega_2 t - \varphi_2) \sum_{m=N_1+1}^N \alpha_m(\bar{E}) \int dE' \sum_{n=1}^{N_1} b_{m\bar{E}, nE'} \alpha_n(E') e^{-iE't} \sum_{k=1}^{N_1} \alpha_k(E') C_{kE'}. \quad (15c)$$

Equation (15b) gives rise to N_1 equations,

$$\begin{aligned} \dot{C}_{nE} = & -iF_1 e^{-i(E_g - E)t} g_1(t) \sin(\omega_1 t - \varphi_1) b_{nE} c_g(t) - iF_2 e^{iEt} g_2(t) \sin(\omega_2 t - \varphi_2) \int dE' \sum_{k=N_1+1}^N b_{nE, kE'} \alpha_k(E') e^{-iE't} \\ & \times \sum_{m=N_1+1}^N \alpha_m(E') C_{mE'}, \end{aligned} \quad (15b')$$

while (15c) gives rise to N_2 equations ($N_1 + N_2 = N$),

$$\dot{C}_{m\bar{E}}(t) = -iF_2 e^{i\bar{E}t} g_2(t) \sin(\omega_2 t - \varphi_2) \int dE' \sum_{n=1}^{N_1} b_{m\bar{E}, nE'} \alpha_n(E') e^{-iE't} \sum_{k=1}^{N_1} \alpha_k(E') C_{kE'}. \quad (15c')$$

We now perform a contour integration in the lower half-plane. Only the poles contribute to the result. Therefore,

$$\int dE' \alpha_m(E') e^{-iE't} \alpha_n(E') \approx \delta_{mn} e^{-iz_n t}, \quad (16)$$

where z_n are the complex poles of $\alpha_n^2(E)$. Thus, assuming the rotating wave approximation (RWA) for every $n \leq N_1$ and $N_1 < m \leq N$ we obtain

$$\dot{c}_g = -\frac{1}{2} e^{-i\varphi_1} F_1 g_1(t) \sum_{n=1}^{N_1} b_{nz_n} e^{i(E_g + \omega_1 - z_n)t} C_{nz_n}, \quad (17a)$$

$$\dot{C}_{nE} = \frac{1}{2} e^{i\varphi_1} F_1 g_1(t) e^{i(E - E_g - \omega_1)t} b_{nE} c_g - \frac{1}{2} e^{-i\varphi_2} F_2 g_2(t) \sum_{k=N_1+1}^N b_{nE, kz_k} e^{i(E + \omega_2 - z_k)t} C_{kz_k}, \quad (17b)$$

$$\dot{C}_{m\bar{E}} = \frac{1}{2} e^{i\varphi_2} F_2 g_2(t) \sum_{k=1}^{N_1} b_{m\bar{E}, kz_k} e^{i(\bar{E} - \omega_2 - z_k)t} C_{kz_k}. \quad (17c)$$

The same procedure, applied to Eq. (7)', results in the form

$$A_{iE}(t) = \sum_n \alpha_n(E) [e^{-iEt} C_{nE}(t) - e^{-iz_n t} C_{nz_n}(t)], \quad (18)$$

where the sum is over the localized components of the i th channel. Note that the sign of ω_2 in Eqs. (17) can be positive or negative, depending on the requirement of the RWA. Here we shall assume that the localized parts of the second channel lie either all above or all below the group of localized parts of the first channel. The solution of Eqs. (17) determines the photoelectron emission amplitudes (18).

In order to perform the time integration in Eqs. (17), the functional dependence on time of the coefficients $C_{nz_n}(t)$ is needed. This implies that their values at the poles z_n are needed. Making the substitution $E \rightarrow z_n$, one obtains a set of equations for $C_{nz_n}(t)$ which are similar to the ones resulting in the case of two groups of bound states, the first being populated from the ground state by the first pulse while the second pulse connects the states of the two groups. In this case, however, both the energies and the dipole matrix elements are real, the latter lacking the part referring to transitions to the continuum.

By inspecting Eqs. (17), we observe that a simpler set of equations is satisfied by the quantities $B_{nz_n}(t) = e^{-iz_n t} C_{nz_n}(t)$ which, as in Ref. [18], are the amplitudes of the localized components of the resonances. These equations are

$$\dot{c}_g = -\frac{1}{2} e^{-i\varphi_1} F_1 g_1(t) \sum_{n=1}^{N_1} b_{nz_n} e^{i(E_g + \omega_1)t} B_{nz_n}, \quad (19a)$$

$$\begin{aligned} \dot{B}_{nz_n} + iz_n B_{nz_n} &= \frac{1}{2} e^{i\varphi_1} F_1 g_1(t) e^{-i(E_g + \omega_1)t} b_{nz_n} c_g \\ &\quad - \frac{1}{2} e^{-i\varphi_2} F_2 g_2(t) \sum_{m=N_1+1}^N b_{nz_n, mz_m} e^{i\omega_2 t} B_{mz_m}, \end{aligned} \quad (19b)$$

$$\dot{B}_{mz_m} + iz_m B_{mz_m} = \frac{1}{2} e^{i\varphi_2} F_2 g_2(t) \sum_{n=1}^{N_1} b_{mz_m, nz_n} e^{-i\omega_2 t} B_{nz_n}, \quad (19c)$$

for every $n \leq N_1$ and $N_1 < m \leq N$.

The assumption of the problem is that the pulse acting on the initial state is ultrashort and relatively weak. Therefore, we take $c_g \approx 1$. (The pulse acting on the initial discrete state is called “first,” although it is not necessarily the first in the temporal order of application.)

Consequently, Eq. (19a) is decoupled from the system of Eqs. (19), and each one of Eq. (19b) now has an inhomogeneous term. This term takes into account the action of the first pulse. For its time envelope, a Gaussian function, $g_1(t) = e^{-\frac{(t-t_a)^2}{2\sigma_a^2}}$, centered at $t = t_a$ is chosen. The envelope of the second pulse, $g_2(t) = e^{-\frac{(t-t_b)^2}{2\sigma_b^2}}$, also a Gaussian, will be approximated by a sum of rectangular functions, each one

composed of two step functions. The step function $\text{St}(t)$ is unity if its argument is positive and zero otherwise. We write

$$g_2(t) \approx \sum_{i=1}^{N_p} g_{2(i)} [\text{St}(t - t_{i-1}) - \text{St}(t - t_i)], \quad (20a)$$

the number of points N_p being an odd number. For the central rectangle, $N_c = \frac{1}{2}(N_p + 1)$, we put $g_{2(N_c)} = 1$, while for $i \neq N_c$, $g_{2(i)} < 1$. If we require the function to be symmetrical, then $g_{2(N_c+k)} = g_{2(N_c-k)}$. The values of $g_{2(i)}$ can be made to

fit any envelope function—a Gaussian $e^{-\frac{(t-t_b)^2}{2\sigma_b^2}}$ in our case—centered at $t = t_b$. This is done in a systematic way in Appendix C of Ref. [18].

We derive the formulas initially for the special case of a single rectangular function:

$$g_2(t) \approx \text{St}(t - t_0) - \text{St}(t - t_1). \quad (20b)$$

The rectangle is centered at t_b , where $t_b = (t_1 + t_0)/2$.

For times $t < t_0$, when $g_2(t)$ is zero, Eqs. (19b) and (19c) for $c_g \approx 1$ can be immediately integrated to give the coefficients C_{nE} . Defining

$$G(E; t_0, t) \equiv \int_{t_0}^t dt' e^{iEt'} g_1(t'), \quad (21)$$

we obtain for $n \leq N_1$

$$C_{nE}(t) = \frac{1}{2} F_1 e^{i\varphi_1} b_{nE} G(E - E_g - \omega_1; -\infty, t), \quad t \leq t_0 \quad (22)$$

for the coefficients referring to the first channel, while the coefficients C_{mE} for $N_1 + 1 \leq m \leq N$, referring to the second channel, are equal to zero.

For times $t_0 < t < t_1$, Eqs. (19b) and (19c) are solved in Appendix A for the case of the rectangular pulse of Eq. (20b). They are expressed in terms of the coupling parameters

$$\Lambda_{nm} = g_2 F_2 b_{nz_n, mz_m}. \quad (23)$$

Although g_2 is, for the time being, equal to unity, it is included in the definition for later purposes.

D. Semianalytic solution for C_{nz_n} when the second pulse is rectangular and extension to the case of an arbitrary temporal shape

The procedure described in Appendix A solves the system of Eqs. (19b) and (19c) for $c_g \approx 1$ in the case of a rectangular second pulse. The solution is written in terms of the integrals $G(E_j; t_0, t)$ of Eq. (21) for $t < t_1$, where the quantities E_j are eigenvalues resulting from the solution of the homogeneous part of the system (19b) and (19c) (see Appendix A). For the chosen Gaussian envelope function $g_1(t)$, the analytic expression of the G integrals is given in terms of the error function (see Appendix B).

In addition to the eigenvalues, one also obtains the matrix of the eigenvectors T and its inverse T^{-1} through which the solution of the system of Eqs. (19) is expressed as

$$e^{-iz_n t} C_{nz_n}(t) = \frac{1}{2} e^{i\varphi_1} F_1 e^{-i(E_g + \omega_1)t} \sum_{j=1}^N T_{nj} e^{-iE_j t} \left(c^{(j)} + G(E_j; t_0, t) \sum_{l=1}^{N_1} T_{jl}^{-1} b_{lz_l} \right), \quad n \leq N_1, \quad (24a)$$

$$e^{-iz_n t} C_{nz_n}(t) = \frac{i}{2} e^{i\varphi_1} F_1 e^{i\varphi_2} e^{-i(E_g + \omega_1 + \omega_2)t} \sum_{j=1}^N T_{nj} e^{-iE_j t} \left(c^{(j)} + G(E_j; t_0, t) \sum_{l=1}^{N_1} T_{jl}^{-1} b_{l z_l} \right), \quad n > N_1, \quad (24b)$$

Note that the second summation in Eqs. (24) has N_1 terms, since Eqs. (19c) have no inhomogeneous term.

The values of the coefficients $c^{(j)}$ are computed by the matching of the solutions Eqs. (22) and (24) at the time $t = t_0$. This is done below for the generalized form of g_2 , which is a sum of rectangular functions of the type introduced in Eq. (20a).

The coefficients $C_{nz_n(i)}(t)$ are computed at each time interval $t_{i-1} \leq t \leq t_i$ of Eq. (20a) in terms of the coupling parameters $\Lambda_{nm(i)} = g_2(i) F_2 b_{nz_m, nz_n}$. The eigenvalues and eigenvectors are calculated at each time interval. Also, the integrals G are calculated with t_{i-1} as the lower bound. The constants $c_i^{(j)}$ at each interval are determined from those of the interval at the left by the continuity conditions $C_{nz_n(i)}(t_{i-1}) = C_{nz_n(i-1)}(t_{i-1})$, where we have set $C_{nz_n(0)}(t) = \frac{1}{2} F_1 e^{i\varphi_1} G(z_n - E_g - \omega_1; -\infty, t) b_{nz_n}$ for $n \leq N_1$, while $C_{nz_n(0)}(t) = 0$ $n > N_1$ for values of time $t < t_0$.

From Eqs. (24) we obtain, in the time interval $t_{i-1} \leq t \leq t_i$,

$$c^{(j)} = e^{iE_j t_{i-1}} \sum_{k=1}^N T_{jk}^{-1} e^{i\beta_k t_{i-1}} e^{-iz_k t_{i-1}} \bar{C}_{k z_k}(t_{i-1}), \quad (25)$$

where,

$$\bar{C}_{nz_n} = \begin{cases} C_{nz_n} / \frac{1}{2} e^{i\varphi_1} F_1, & n \leq N_1 \\ C_{nz_n} / \frac{i e^{i\varphi_2}}{2} e^{i\varphi_1} F_1, & n > N_1 \end{cases}$$

and

$$\beta_n(t) = \begin{cases} E_g + \omega_1, & n \leq N_1 \\ E_g + \omega_1 + \omega_2, & n > N_1 \end{cases}. \quad (26)$$

Combining Eqs. (24) and (25), one obtains for $t_{i-1} \leq t \leq t_i$

$$e^{-iz_n t} \bar{C}_{nz_n}(t) = e^{-i\beta_n t} \sum_{k=1}^N \left[\sum_{j=1}^N T_{nj} e^{-iE_j(t-t_{i-1})} T_{jk}^{-1} \right] e^{i\beta_k t_{i-1}} e^{-iz_k t_{i-1}} \bar{C}_{k z_k}(t_{i-1}) + e^{-i\beta_n t} \sum_{l=1}^{N_1} \left[\sum_{j=1}^N T_{nj} e^{-iE_j t} G(E_j, t_{i-1}, t) T_{jl}^{-1} \right] b_{l z_l}. \quad (27)$$

The quantity in the first square brackets is the time evolution operator $U_{nk}(t - t_{i-1})$ while the second term describes the population of the localized components due the first pulse $g_1(t)$. Since the first pulse is ultrashort, the G integrals fall quickly to zero.

Therefore, Eq. (27) describes the evolution of the amplitudes of the localized components of the resonances under the influence of the second pulse.

E. Final results for the two ionization channels

With the form of the coefficients C_{nz_n} known, Eqs. (17b) and (17c) are integrated in the region $t_0 \leq t' < t$, with the restriction $t \leq t_{N_p}$, and the expressions for the coefficients $C_{nE}(t)$ are obtained as

$$C_{nE}(t) = \frac{1}{2} e^{i\varphi_1} F_1 b_{nE} G(E - E_g - \omega_1, t_0, t) - \frac{i}{4} e^{i\varphi_1} F_1 F_2 \sum_{m=N_1+1}^N b_{nE, m z_m} \int_{t_0}^t dt' g_2(t') e^{i(E + \omega_2 - z_m)t'} \bar{C}_{m z_m}(t') \quad (28a)$$

for $n \leq N_1$, and

$$C_{mE}(t) = \frac{1}{4} e^{i\varphi_1} F_1 e^{i\varphi_2} F_2 \sum_{n=1}^{N_1} b_{mE, n z_n} \int_{t_0}^t dt' g_2(t') e^{i(E - \omega_2 - z_n)t'} \bar{C}_{n z_n}(t') \quad (28b)$$

for $m > N_1$.

It is convenient to write the integrals in Eqs. (28) in a compact form, in terms of the parameter β . Thus, assuming the form (20a), for $g_2(t)$ one has, at a certain time $t \leq t_p$,

$$\sum_{i=1}^p g_2(i) \int_{t_{i-1}}^t dt' e^{i(E - \beta_n)t'} e^{-i(z_m - \beta_m)t'} \bar{C}_{m z_m}(t'), \quad \text{for } p \leq N_p$$

where n and m belong to *different* groups of localized components. Substituting the value of $e^{-i(z_m - \beta_m)t} \bar{C}_{m z_m}(t)$ from Eq. (27), one obtains for the reduced coefficients \bar{C}_{nE}

$$\bar{C}_{nE}(t) = b_{nE} G(E - E_g - \omega_1, t_0, t) - F_2 \sum_{m=N_1+1}^N b_{nE, m z_m} P_{mE}^n(t) \quad (29a)$$

for $n \leq N_1$ and

$$\bar{C}_{mE}(t) = -F_2 \sum_{n=1}^{N_1} b_{mE, n z_n} P_{nE}^m(t) \quad (29b)$$

for $m > N_1$, where

$$P_{mE}^n(t) = \frac{1}{2} \sum_{i=1}^p g_{2(i)} \sum_{k=1}^N \left[\sum_{j=1}^N T_{mj} \frac{e^{i(E-\beta_n)t} e^{-iE_j(t-t_{i-1})} - e^{i(E-\beta_n)t_{i-1}}}{(E-\beta_n-E_j)} T_{jk}^{-1} \right] e^{i\beta_k t_{i-1}} e^{-iz_k t_{i-1}} \bar{C}_{kz_k}(t_{i-1}) \\ + \frac{1}{2} \sum_{i=1}^p g_{2(i)} \sum_{l=1}^{N_1} \left[\sum_{j=1}^N T_{mj} \frac{e^{i(E-\beta_n-E_j)t} G(E_j, t_{i-1}, t) - G(E-\beta_n, t_{i-1}, t)}{(E-\beta_n-E_j)} T_{jl}^{-1} \right] b_{lz_l} \quad (30)$$

for $t \leq t_p$.

Equations (29) express the generalization of the corresponding result obtained in Ref. [18] for the simple case $N_1 = N_2 = 1$. For $t > t_{N_p}$, i.e., after the end of the last time segment at $t = t_{N_p}$, the integrals reach a constant value. The spectral asymmetry functions b_{nE} and $b_{nE, m z_m}$ can be expressed in terms of q parameters, the former being the usual Fano q parameter and the latter being a complex one, introduced in Ref. [18]. It refers to a resonant to resonant transition, and it is expressed in terms of the Q parameter and the branching ratios $\gamma^{(1)}$ and $\gamma^{(2)}$ for that transition [see the discussion after Eqs. (10) and (11)]. It is given by $q_{nm} = (Q_{nm} - i\gamma_{nm}^{(2)})/\gamma_{nm}^{(1)}$ for the coefficients of the first channel and $q_{mn} = (Q_{nm} - i\gamma_{nm}^{(1)})/\gamma_{nm}^{(2)}$ for those of the second channel. Note that the q parameter for the transition $m \rightarrow n$ is different from the parameter for the transition $n \rightarrow m$.

It must be noted that the importance of Fano's q parameter is based on the fact that $G(E - \beta_n, t_0, t)$ is a simple function of the energy. On the other hand, the functions $P_{nE}^m(t)$ have, in general, a rich and often complicated structure, where the importance of q_{nm} is reduced drastically.

The reduced coefficients \bar{C}_{nE} , given by Eqs. (29), together with their values $\bar{C}_{n z_n}$ at the poles z_n , given by Eq. (27), are now used to evaluate the ionization probability amplitudes $A_{iE}(t)$ of Eq. (18) for each channel.

As it can be seen from Eq. (30), the results are sensitive to the exact position of the complex poles (i.e., energies and half-widths), which determine the eigenvalues E_j appearing in the denominators of the expression. The results are also sensitive, in an indirect way, to the time delay, t_D , which determines the relative position of the peaks of the two pulses. In the calculations, the peak t_b of the second pulse $g_2(t)$ was set arbitrarily to zero. With this convention, the peak t_a of the first pulse $g_1(t)$ is equal to the time delay t_D . Notice that g_1 is contained in the G integral, defined in Eq. (21), and whose form, in the case of a Gaussian pulse, is given in Appendix B. This integral appears in Eq. (30), as well as in Eq. (27), where the quantities $\bar{C}_{n z_n}(t)$ are calculated.

F. Extension to many angular momenta for each parity

Let there be I_1 channels with parity opposite to that of the ground, or initial discrete, state of angular momentum L , and let I_2 be channels with parity opposite to that of the previous group. The dipole selection rules are assumed so that

$I_1 \leq 3$ and $I_2 \leq 5$. The summation in Eq. (1) now contains two groups of channels, the members of each being coupled to the members of the other by dipole transitions. Let there be N_i resonance states at the i th ionization channel of a given total angular momentum and parity.

As in the case of two channels, a numbering of the channels and resonances taken into account is required in order to avoid double indices. Conventionally, the numbering starts from the lowest angular momentum of the first group of channels having parity opposite to that of the ground state. Then, in the same way, the channels and resonances of the second group are numbered. Let us define the cumulative quantities

$$M_i = \sum_{j=1}^i N_j.$$

The resonances of the i th channel are then counted from $M_{i-1} + 1$ up to $M_i \equiv M_{i-1} + N_i$ with the convention $M_0 = 0$. The formulas of the previous sections are then modified accordingly. Thus, for example, the transformation of Eqs. (14) becomes

$$c_{iE} = \sum_{n=M_{i-1}+1}^{M_i} \alpha_n(E) C_{nE},$$

while the summations in the Eqs. (17) are modified in the same way. The number of Eqs. (17) is now greater, but the extension is straightforward and Eq. (18) referring to the final quantities $A_{iE}(t)$ remains unaltered.

III. APPLICATION TO THE MANY-ELECTRON CASE OF THE CARBON K -EDGE IONIZATION BY AN ATTOSECOND PULSE

The formalism solves the problem of N_1 resonances in a scattering channel populated from the ground state by an ultrashort, and consequently spectrally broad, initial pulse, followed by a longer second pulse that transfers populations to N_2 resonances in a second scattering channel. The degree of population transfer due to the second pulse between the two sets of resonances (back and forth) depends mainly on the size of the transition moment, on the intensity of the second pulse, and on the amount of detuning from exact resonance.

A. Essential elements of the calculation of wave functions

In the present first implementation of the multistate theory, we have chosen the case $N_1 = 2$, $N_2 = 1$. It involves the K -shell photoexcitation of carbon $1s^2 2s^2 2p^2 \ ^3P$ interacting with two ultrafast pulses, according to the general scheme A. As explained in the Introduction, the possibility of acquiring spectroscopic information about the excitation of carbon at the K edge via scheme A is significant to both experiment and theory.

Because of the extreme complexity that results when considering all possible excitations, states, and open channels, judicious selections were made, allowing the reduction of the size of the many-electron, many-channel problem while obtaining semiquantitative information on observable spectral features for realistic pulses. From a series of trial calculations, we concluded that the results are sensitive to the values of the transition moments as well as to the autoionization widths. Therefore, the focus was on the prediction of observable phenomena in a qualitative manner, rather than on the determination of detailed data that are numerically very accurate.

The chosen excitation-coupling scheme is as follows: The first (attosecond) pulse prepares a superposition of $1\bar{s}2\bar{s}^2 2\bar{p}^3$ and $[1\bar{s}2\bar{s}^2 (2\bar{p}^2 \ ^3P) \ ^4P] 3\bar{p}$ states of $^3S^0$ symmetry. In other words, we consider only the $^3S^0$ excited symmetry, with the superposition consisting of two resonance states, one representing $1s$ -electron excitation reaching the vacant $2p$ valence shell and the other representing $1s$ -electron excitation reaching the vacant $3p$ Rydberg shell. These two core-hole states of carbon are embedded in a number of open channels. The Hartree-Fock (HF) orbitals of the zero-order configurations are state-specific. They are calculated in their own self-consistent potential, which is influenced by the presence of the hole in the $1s$ shell.

As regards the mixing of symmetry-adapted configurations representing electron correlation and the availability of open channels, the $^3S^0$ symmetry cannot be retained by the substitutions $2\bar{p}^2 \rightarrow 1s\epsilon s$ or $2\bar{p}3\bar{p} \rightarrow 1s\epsilon s$. So, at the level of pair correlations, the open-channel configurations possible arise from the substitutions, $2\bar{s}3\bar{p} \rightarrow 1s\epsilon p$, $2\bar{s}2\bar{p} \rightarrow 1s\epsilon p$ or $2\bar{s}^2 \rightarrow 1s\epsilon s$. From these, the last one was neglected as it is expected to have the least contribution to the total width. The first two lead to the $1s^2 2\bar{s} (2\bar{p}^2 \ ^3P) \ ^4P \epsilon \bar{p}^3 S^0$ ionization channel, which contains the two resonances of $^3S^0$ symmetry. Note that the calculation of the coupling matrix elements must account for *nonorthonormality* (NON), as the orbitals in the presence of the core hole differ from those in its absence (i.e., $\langle 1s|2\bar{s}\rangle \neq \langle 1\bar{s}|2s\rangle \neq 0$).

The second pulse, ω_2 , couples the superposition of the two $^3S^0$ resonances to the $[1\bar{s}2\bar{s}^2 (2\bar{p}^2 \ ^3P) \ ^4P] 3d \ ^3P$ autoionizing state (Fig. 1). In zero order, the one-electron dipole transitions are $2p \rightarrow 3d$ and $3p \rightarrow 3d$, the latter having a much larger transition amplitude.

The $3d \ ^3P$ $1s$ -hole state autoionizes to a number of open channels, of which the most important is the $1s^2 2s^2 2p\epsilon p \ ^3P$. This results from the interaction of the pair $2p3d \rightarrow 1s\epsilon p$. This channel is directly populated via electric dipole transitions from the two $^3S^0$ resonances. These transitions are dominated by the matrix elements, $\langle 1s|r|2\bar{p}\rangle \langle 2\bar{p}|\epsilon p\rangle$ for the valence configuration $1s2s^2 2p^3 \ ^3S^0$ and $\langle 1s|r|2\bar{p}\rangle \langle 3\bar{p}|\epsilon p\rangle$ and

$\langle 1s|r|3\bar{p}\rangle \langle 2\bar{p}|\epsilon p\rangle$ for the Rydberg configuration $1s2s^2 2p^2 3p \ ^3S^0$.

Also, the $1s^2 2\bar{s} (2\bar{p}^2 \ ^3P) \ ^4P \epsilon \bar{p}^3 S^0$ channel, is populated via dipole transitions from the 3P resonant state by the $3d \rightarrow \epsilon p$ transition as well as from the ground state by the $2s \rightarrow \epsilon p$ transition. The former is effected because of the nonzero overlap ($1\bar{s}|2s$). The contribution of the latter is small because of the large energy of the outgoing electron.

Another open channel for autoionization of the $3d$ resonance state is the $1s^2 2s^2 3d\epsilon d \ ^3P$, corresponding to the rearrangement $2p^2 \rightarrow 1s\epsilon d$. However, in first order, it has zero matrix element with the state $[1\bar{s}2\bar{s}^2 (2\bar{p}^2 \ ^3P) \ ^4P] 3d$ because of the 3P internal coupling of the pair $2p^2$, even though, due to NON, there is a small nonzero matrix element. The autoionization coupling to the $1s^2 2s^2 3d\epsilon d \ ^3P$ channel was neglected.

The calculation of the bound wave functions was done in the spirit of the *state-and property-specific approach* to the solution of problems of many-electron physics (see Refs. [13,17,25–27] and references therein). The zero-order descriptions were obtained at the level of the HF or multiconfigurational HF (MCHF) approximations, for both the discrete and the resonance states. The scattering orbitals were obtained in the term-dependent frozen core of the corresponding channel. Only selected portions of electron correlations were considered. For example, for the carbon 3P ground state, we started with a MCHF $1s^2 2s^2 2p^2 + 1s^2 2p^4$ wave function, calculated numerically, and added electron correlation terms corresponding to virtual excitations from the $2s$ and $2p$ shells that were optimized variationally. For the excited $^3S^0$ states, we started with a $1s2s^2 2p^3 + 1s2s2p^3 3s$ MCHF zero-order wave function for the first resonance, and a $1s2s^2 2p^2 3p + 1s2p^4 3p + 1s2s^2 2p^3$ MCHF zero order wave function for the second resonance. To these, the most significant double virtual excitations from the $2p$ subshell were added. Finally, for the excited 3P state, we started with a $1s2s^2 2p^2 3d + 1s2p^4 3d$ MCHF zero-order wave function and added the most significant double virtual excitations from the $2p$ subshell. The correlation between the Rydberg MCHF orbitals, $3p$ and $3d$, and the core orbitals were neglected.

An important set of parameters for the qualitative understanding of the phenomena that result from scheme A is the magnitude of the transition matrix elements. For the chosen case of carbon, the matrix element pertaining to the dipole transition from the ground state to the first localized part of the first channel, d_{g1} , is about five times greater than the corresponding quantity from the ground state to the second localized part of the same channel, d_{g2} . This is a common pattern, since at the lower end of Rydberg series often lies a valence state which is as compact as the ground one and the dipole coupling between them is higher than the coupling between the ground state and the extended Rydberg ones.

On the other hand, the dipole transition matrix element from the second localized part of the first channel to the localized part of the second channel, d_{23} , is about 40 times greater than the corresponding quantity from the first localized part, d_{13} . This is not surprising since the two Rydberg levels have the same principal quantum numbers, and, as is known from the hydrogenic spectra, these have the largest dipole

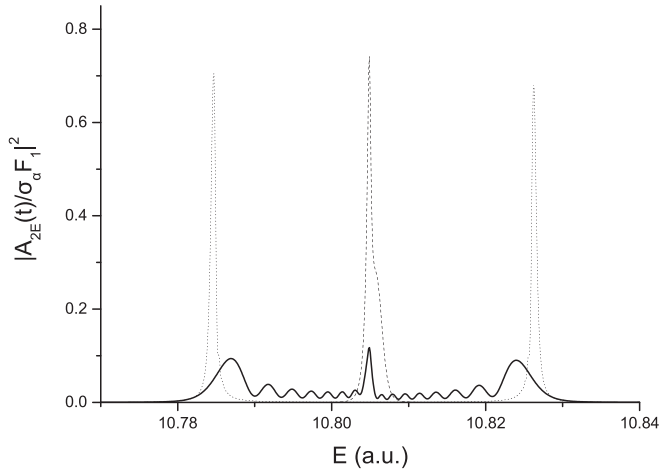


FIG. 2. The reduced ionization probability $|A_{2E}(t)/\sigma_a F_1|^2$ (in a.u.), as a function of energy E (in a.u.) above the carbon ground state, $1s^2 2s^2 2p^2 \ ^3P$, for a time t where the two Gaussian pulses are essentially zero. The pulses $g_1(t)$ and $g_2(t)$ have full widths at half maximum of 100 as and 80 fs, and intensities $I_1 = 5 \times 10^{11}$ W/cm² and $I_2 = 5 \times 10^{12}$ W/cm², respectively. $A_{2E}(t)$ corresponds to the second channel $1s^2 2s^2 2p \epsilon p \ ^3P$, and the energy E is in the vicinity of the E_3 [$1s^2 2s^2 2p^2 ({}^4P) 3d \ ^3P$] resonance state. The frequency of the first pulse is chosen to be $\omega_1 = 10.76$ a.u., which excited resonantly the E_2 ($1s^2 2s^2 2p^2 3p \ ^3S^o$) resonance state. The curve with solid line corresponds to $t_{FWHM} = 80$ fs. The dotted line corresponds to $t_{FWHM} = 2000$ fs. The dashed line corresponds to $t_{FWHM} = 80$ for a weaker intensity, namely, 400 times smaller than the value of I_2 .

couplings. Consideration of such data is critical when analyzing field-induced electron dynamics.

We define the *reduced* ionization probability densities $|A_{iE}(t)/\sigma_a F_1|^2$, derived from Eqs. (18) and (28), in order to remove the common factors with the characteristics of the first pulse. The remaining part has a slight dependence on the standard deviation of the first Gaussian pulse, σ_a , which is indicated by Eqs. (B2)–(B3) of the Appendix B (see also Ref. [29]). This is the quantity plotted in Figs. 2–4.

We chose the energies of the two pulses such that their sum equals the energy difference between the ground state and the 3P Rydberg resonance of the second channel, i.e., $\omega_1 + \omega_2 = E_3 - E_{gs} = 10.81$ a.u. = 294.1 eV. The energies of the two resonances of ${}^3S^o$ symmetry were calculated to be about 10.46 a.u. (284.6 eV) (the core-hole valence $1s^2 2s^2 2p^3 \ ^3S^o$) and 10.76 a.u. (292.8 eV) (the core-hole Rydberg $1s^2 2s^2 2p^2 3p \ ^3S^o$), above the ground state. In the calculations we varied the energy of the first pulse so as to scan the interval between the energies of these two resonances, while satisfying the condition for the two-pulse excitation stated above, $\omega_1 + \omega_2 = E_3 - E_{gs} = 10.81$ a.u. = 294.1 eV. Since the resonance of the second channel lies slightly above the second resonance of the first channel, by about 1.3 eV, the energy of the second pulse lies in the range of the near-infrared to visible.

Below we present the results that correspond to the following two pulses. The first, high-frequency, attosecond pulse has full width at half maximum (intensity) $t_{FWHM} = 2\sqrt{\ln 2} \sigma_a / 100$ as (σ_a is the standard deviation of the Gaussian, $\exp[-(t - t_a)^2 / 2\sigma_a^2]$), and intensity

$I_1 = 5 \times 10^{11}$ W/cm² (field strength, $F_1 = 1.7 \times 10^{-2} / \sqrt{20}$ a.u.). The second, low-frequency, femtosecond pulse has intensity $I_2 = 5 \times 10^{12}$ W/cm² ($F_2 = 1.7 \times 10^{-2} / \sqrt{2}$ a.u.) and t_{FWHM} 80 fs. The values for the second pulse were chosen after a number of test calculations for higher intensities (up to 10^{13} W/cm²) and lower widths (20 fs).

For the energy difference between the two Rydberg resonances, $3p \ ^3S^o - 3d \ ^3P$, $\omega_2 \sim 1.3$ eV, and the corresponding number of field cycles is about 30. Notice that the corresponding FWHM of the second pulse in the energy spectrum is 32 meV, much smaller than the distance to the next member of the nd Rydberg series which lies 680 meV higher. This narrow width justifies the inclusion of only one resonance in the second ionization channel.

Figure 2 shows results that have to do with the well-known Autler-Townes splitting of ac-field physics, due to the coupling between the $3p \ ^3S^o$ and $3d \ ^3P$ resonances. We are looking at the second channel, where the $3d \ ^3P$ resonance is found. The two frequencies are on resonance with the $3p \ ^3S^o$ and $3d \ ^3P$ states. The dotted line curve corresponds to a weak field, namely, 0.05 times smaller than the value of F_2 stated above, with the second pulse having t_{FWHM} of 80 fs. In this case, only one peak appears at 10.81 a.u.. When the field strength increases to F_2 , with the pulse having again the t_{FWHM} of 80 fs, the reduced ionization probability density is divided into three main peaks (plus small side bands of interference), the two additional ones corresponding to the Autler-Townes splitting which starts emerging (thick solid black line). This deviation from the normal ac result is due to the fact that the fields are short Gaussian pulses and not of the ac type. Indeed, in order to explore this possibility, we did a calculation for an extremely long pulse, having t_{FWHM} of 2000 fs, in order to simulate the situation of an ac field. The corresponding results (dashed line curve) show only two peaks, as expected from the theory with ac fields. In contradistinction, a single peak appears when the pulse is chosen to have a small t_{FWHM} , such as 20 fs. (For reasons of economy we do not include this result in the figure.)

Figure 3 is about the effects of interference in the first channel as a function of the time delay. It displays the results of two types of calculation, with the pulses being on resonance, for various values of time delay t_D . The narrow black line corresponds to the case where both pulses act simultaneously. The wiggles result from the interference in the coupling $3p \ ^3S^o \leftrightarrow 3d \ ^3P$. Indeed, when the second pulse is taken out, the curve changes to that depicted by the smooth thick gray line. In Fig. 3 it is shown the trend of the gradual disappearance of interference as time delay goes to large negative values (the short XUV pulse peaks *before* the second pulse) and to large positive ones (the short XUV pulse peaks *after* the second pulse).

Figure 4 shows results that demonstrate the necessity of dealing with superpositions of resonance states when using spectrally broad pulses. In the lower plot of Fig. 4 the first pulse is close (10.48 a.u.) to the first resonance, $2p^3 \ ^3S^o$. The second pulse connects with the $3d \ ^3P$ state resonantly. The time delay is zero, and the second pulse has the duration of 80 fs. We focus on the second channel. Two types of results are compared: one which includes the superposition of the ${}^3S^o$ resonances and one where the Rydberg state $1s^2 2s^2 2p^2 3p \ ^3S^o$,

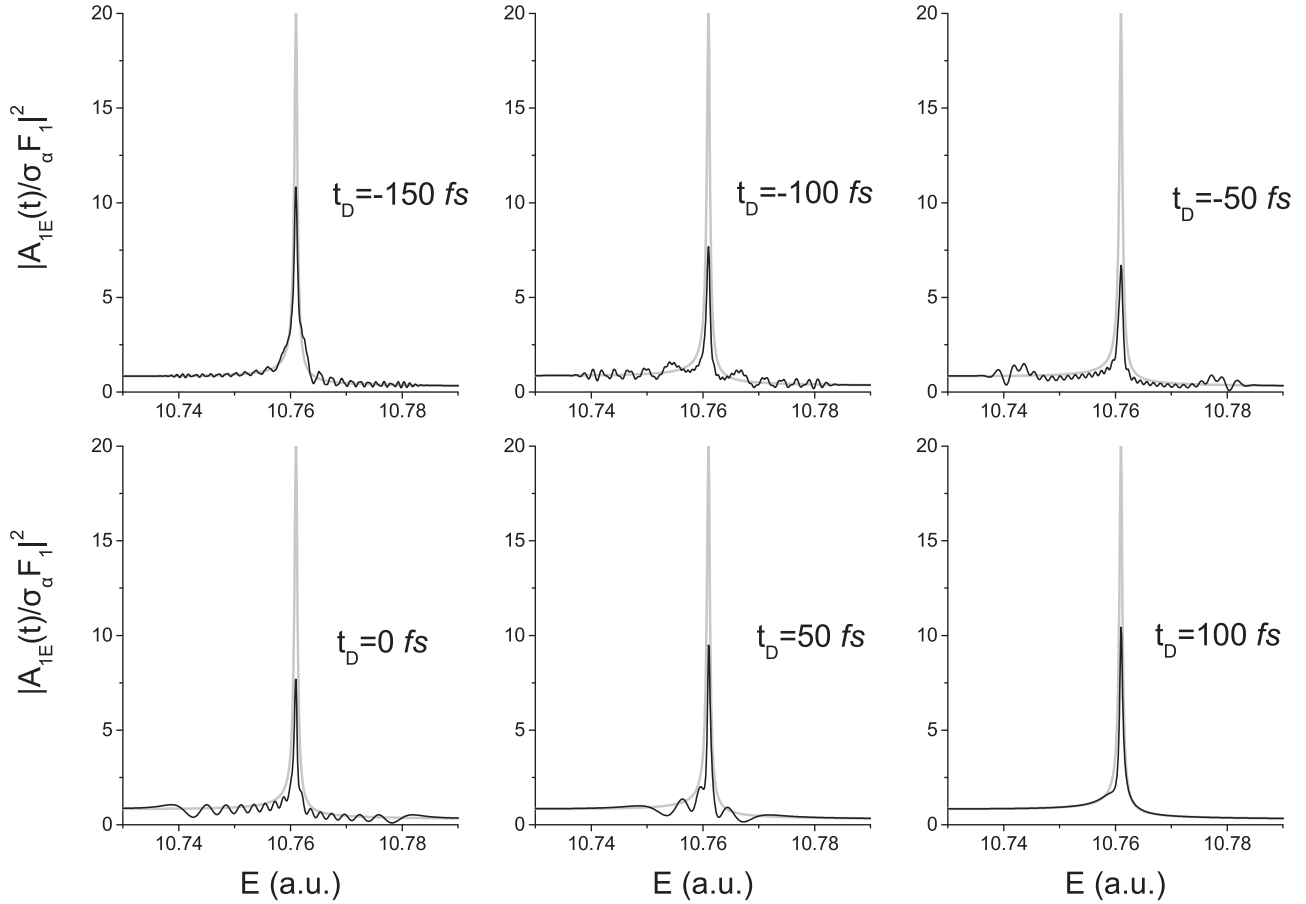


FIG. 3. The reduced ionization probability $|A_{1E}(t)/\sigma_{\alpha} F_1|^2$ (in a.u.) as a function of energy E (in a.u.) above $C 1s^2 2s^2 2p^2 \ ^3P$, for a time t where the two Gaussian pulses are essentially zero. The pulses $g_1(t)$ and $g_2(t)$ have full widths at half maximum of 100 as and 80 fs, and intensities $I_1 = 5 \times 10^{11}$ W/cm² and $I_2 = 5 \times 10^{12}$ W/cm², respectively. $A_{1E}(t)$ corresponds to the first channel $1s^2 2s^2 2p^2 \epsilon p \ ^3S^o$, and the energy E is in the vicinity of the $E_2 (1s^2 2s^2 2p^2 3p \ ^3S^o)$ resonance, which is strongly coupled to the $E_3 (1s^2 2s^2 2p^2 (^4P) 3d \ ^3P)$ resonance state by the pulse of frequency ω_2 and temporal shape $g_2(t)$. In this case, the frequency of the first pulse is chosen to be $\omega_1 = 10.76$ a.u., which excites resonantly the $E_2 (1s^2 2s^2 2p^2 3p \ ^3S^o)$ inner-hole state. Consequently, the frequency of the second pulse is $\omega_2 = 0.045$ a.u. (see Fig. 1). Results are shown for time delays, t_D , between -150 fs and $+100$ fs. The thick gray curves correspond to the quantity $|A_{1E}(t)/\sigma_{\alpha} F_1|^2$ that is calculated in the absence of the second pulse ($I_2 = 0$ W/cm²).

is excluded, implying, incorrectly, that the pulse is not broad enough to cover both $^3S^o$ resonances. In the former case (thick black line), the theory produces, correctly, three lines, at energies $E_1 + \omega_2$, $E_2 + \omega_2$, and E_3 . In the latter case (dotted line), the result of the calculation is incorrect, since the line $E_2 + \omega_2$ is absent.

It is expected that the semiquantitative phenomenology suggested by these results can be tested in appro-

appropriate measurements of photoelectron spectra at different energies.

IV. CONCLUSION

We have solved formally as well as computationally, for the case of the carbon K -edge excitation, the problem stated in the Introduction and depicted by the pump-probe scheme A:

$$|0\rangle \xrightarrow[\text{atto sec pulse } \omega_1]{\text{weak}} (\text{superposition of resonances}) \xleftrightarrow[\text{femtosec pulse } \omega_2]{\text{moderately strong}} (\text{superposition of resonances}). \quad (\text{A})$$

This is a time-dependent many-electron problem, involving the two-color excitation by spectrally broad ultrafast pulses of *superpositions of resonances* in the continuous spectra of atoms and molecules. In accordance with current research on the theoretical and experimental study of time-resolved electron dynamics, the chosen duration of the two pulses

ranges from a few decades of femtoseconds to a few decades of attoseconds.

The theory is time-dependent, and its solution was achieved mainly analytically. Its computational implementation is extremely economic. The numerical demonstration involved the two-color excitation and coupling by Gaussian

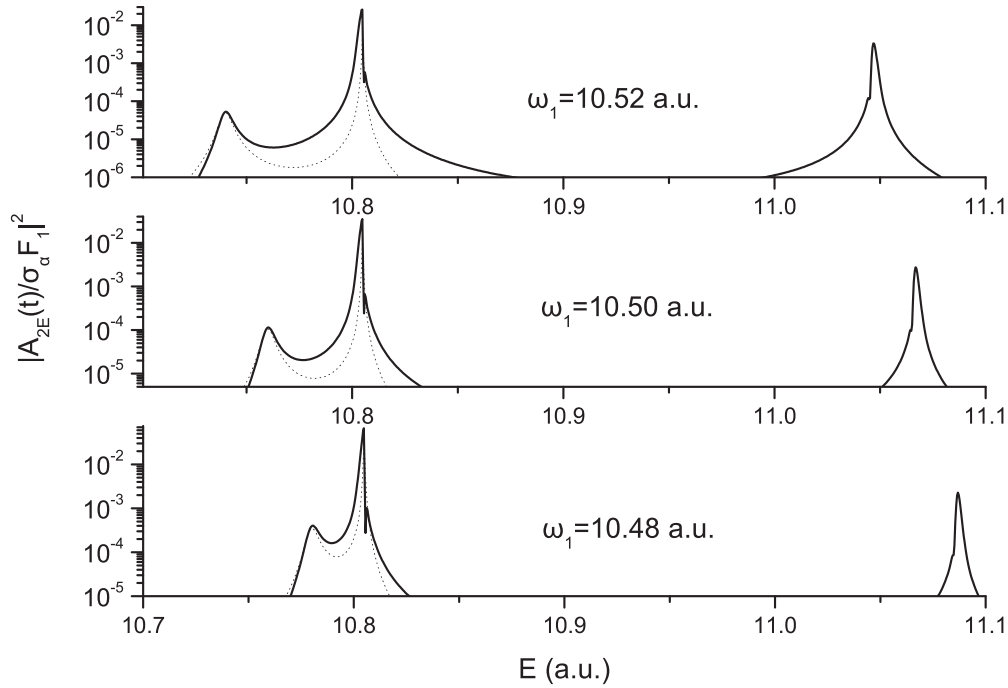


FIG. 4. The reduced ionization probability $|A_{2E}(t)/\sigma_a F_1|^2$ (in a.u.) as a function of energy E (in a.u.) above C $1s^2 2s^2 2p^2 \ ^3P$, for a time t where the two Gaussian pulses are essentially zero. $A_{2E}(t)$ corresponds to the second channel, $1s^2 2s^2 2p \ \epsilon p \ ^3P$, and the energy E is in the vicinity of the E_3 ($1s^2 2s^2 2p^2 (^4P) 3d \ ^3P$) resonance state. Results are shown (solid line curves), for three values of the frequency ω_1 , (given in the figure), which bring the excitation just above the E_1 ($1s^2 2s^2 2p^3 \ ^3S^o$) resonance state. The dotted line curves correspond the same quantity by omitting the E_2 ($1s^2 2s^2 2p^2 3p \ ^3S^o$) resonance state from the calculations, i.e., by incorrectly ignoring the superposition prepared by the attosecond pulse.

pulses of core-excited autoionizing states of carbon near the K edge, as displayed in Fig. 1 and explained in Secs. I and III.

It was determined that the results, whose main features are discussed in Sec. III, have a sensitive dependence on the values of the autoionization widths and on the central frequencies of the pulses. For a given set of intensity, frequency, and duration of the second pulse, the system was also studied as a function of the *time delay*, t_D , in the application of the two pulses, which is a practical control parameter. The results are displayed in Figs. 2–4.

The multiresonance formalism has generalized the *discrete-resonance-resonance* single-state time-dependent excitation and coupling theory that was published recently [18]. Its implementation herein involved two open channels and led to explicit formulas for the time-dependent probability amplitude, $A_{iE}(t)$, $i = 1, 2$, of photoionization into each of the two channels [Eq. (18)].

The basis of our approach is the expansion of the total time-dependent wave function in terms of the stationary discrete and resonance states on the real energy axis, so that the field-free Hamiltonian is diagonal within each angular momentum subspace. Accordingly, suitable mathematical analysis leads to the simplicity of Eqs. (17), where the time-dependent coefficients, $C_{nE}(t)$, of the eigenstates depend solely on their values at the complex energies (z_n) of the resonances, i.e., $C_{nz_n}(t)$. At the core of the methodology is the derivation of an analytic expression for the operator which describes the time evolution of $C_{nz_n}(t)$; see Eq. (27) and related discussion.

Consequently, the time integrals in Eqs. (28), which provide the $C_{nE}(t)$, are also evaluated analytically. This fact

allows their extremely fast evaluation, even on small computers, once the necessary *many-electron* wave functions and matrix elements have been calculated. Running a sufficient number of calculations for different values of the parameters of the two pulses poses no problems in regard to the required computer power and the time of computation. Once the relevant N -electron matrix elements have been calculated, complete calculations for a given set of pulse parameters can be executed on a few-seconds timescales. Therefore, provided reliable N -electron wave functions are computable, as is our case, it becomes possible to acquire a good understanding of the dynamics of scheme A for each system of interest and for a wide range of pulse parameters.

APPENDIX A

Written in terms of the coupling parameters Λ_{mn} , the system of equations satisfied by the variables $B_{nz_n}(t) = e^{-iz_n t} C_{nz_n}(t)$ is

$$\begin{aligned} \dot{B}_{nz_n} + iz_n B_{nz_n} &= \frac{1}{2} e^{i\varphi_1} F_1 g_1(t) e^{-i(E_g + \omega_1)t} b_{nz_n} \\ &\quad - \frac{1}{2} e^{-i\varphi_2} e^{i\omega_2 t} \sum_{m=N_1+1}^N \Lambda_{nm} B_{mz_m}, \end{aligned} \quad (\text{A1a})$$

$$n \leq N_1,$$

$$\dot{B}_{mz_m} + iz_m B_{mz_m} = \frac{1}{2} e^{i\varphi_2} e^{-i\omega_2 t} \sum_{n=1}^{N_1} \Lambda_{mn} B_{nz_n}, \quad (\text{A1b})$$

$$m > N_1.$$

This is an inhomogeneous system of linear differential equations for the amplitudes of the localized components of the resonances. The exponential factors $e^{\pm i\omega_2 t}$ are removed from the second terms of (A1a) and (A1b) by the transformation

$$B_{n z_n}(t) = x_n(t) e^{-i(E_g + \omega_1)t} \quad n \leq N_1, \quad (\text{A2a})$$

$$B_{m z_m}(t) = i e^{i\varphi_2} x_m(t) e^{-i(E_g + \omega_2 + \omega_2)t}. \quad m > N_1 \quad (\text{A2b})$$

The common factors $e^{-i(E_g + \omega_1)t}$ can have any value. However, with this choice the formulas are expressed naturally in terms of the appropriate energy differences. The new dependent variables satisfy the equations

$$\begin{aligned} \dot{x}_n = & -i(z_n - E_g - \omega_1)x_n - \frac{i}{2} \sum_{m=N_1+1}^N \Lambda_{nm} x_m \\ & + \frac{1}{2} e^{i\varphi_1} F_1 g_1(t) b_{n z_n}, \end{aligned} \quad (\text{A3a})$$

$$\dot{x}_m = -i(z_m - E_g - \omega_1 - \omega_2)x_m - \frac{i}{2} \sum_{n=1}^{N_1} \Lambda_{mn} x_n. \quad (\text{A3b})$$

The system (A3) now has the general form $\dot{\underline{x}} = -iA\underline{x} + \underline{f}$ where

$$A = \begin{pmatrix} D^{(1)} & \frac{1}{2}\Lambda \\ \frac{1}{2}\tilde{\Lambda} & D^{(2)} \end{pmatrix}. \quad (\text{A4})$$

This is a block matrix where D_1 and D_2 are *diagonal* square matrices of dimensions $N_1 \times N_1$ and $N_2 \times N_2$, respectively, with matrix elements $D_n^{(1)} = z_n - E_g - \omega_1$ and $D_m^{(2)} = z_m - E_g - \omega_1 - \omega_2$. The quantity Λ is an $N_1 \times N_2$ matrix containing the coupling parameters defined in Eq. (21) with $\tilde{\Lambda}$ its transpose. The inhomogeneous term has only N_1 components.

Following the standard procedure, the solution is found by putting $\underline{x}(t) = \underline{x}_0 e^{-iEt}$. Then, excluding the inhomogeneous term, the system (A3) becomes a time-independent homogeneous system of N equations which is solved as a *complex eigenvalue* problem $A\underline{x}_0 = E\underline{x}_0$.

The general solution of the homogenous system is, $\underline{x}(t) = \sum_j c_j \underline{x}_0^{(j)} e^{-iE_j t}$. A complex diagonalization subroutine is required to produce the complex eigenvalues E_j and eigenvectors $\underline{x}_0^{(j)}$ of A . The general solution of the inhomogeneous system consists of the general solution of the homogeneous system plus a particular solution of the inhomogeneous one. The latter is found by the following procedure.

The matrix A is diagonalized by the similarity transformation $T^{-1}AT = A_d$, where the matrix T contains in its columns the eigenvectors, and the diagonal matrix A_d contains the eigenvalues. Thus, the inhomogeneous system can be written as $\dot{\underline{x}} = -iT A_d T^{-1} \underline{x} + \underline{f}$, and, putting $\underline{y} = T^{-1} \underline{x}$ and $\underline{h} = T^{-1} \underline{f}$, we obtain the equivalent system $\dot{\underline{y}} = -iA_d \underline{y} + \underline{h}$. Since A_d is a diagonal matrix, the equations of the equivalent system are decoupled and can be solved by standard methods. The solution has the form

$$y_j = c_j e^{-iE_j t} + e^{-iE_j t} \int_{t_0}^t dt' e^{iE_j t'} h_j(t'). \quad (\text{A5})$$

Note that the last N_2 components of \underline{f} are zero, since Eqs. (A3b) have no inhomogeneous term. Through the definition

of the integral $G(E, t_0, t)$ [Eq. (21)] we may write

$$y_j = c_j e^{-iE_j t} + \frac{1}{2} e^{i\varphi_1} F_1 e^{-iE_j t} G(E_j, t_0, t) \sum_{k=1}^{N_1} T_{jk}^{-1} b_{k z_k}. \quad (\text{A6})$$

When multiplied by T , the first term produces the general solution of the homogeneous system, while the second term produces a particular solution of the inhomogeneous one. Therefore,

$$x_n = \frac{1}{2} e^{i\varphi_1} F_1 \sum_{j=1}^N T_{nj} e^{-iE_j t} \left(c^{(j)} + G(E_j, t_0, t) \sum_{k=1}^{N_1} T_{jk}^{-1} b_{k z_k} \right), \quad (\text{A7})$$

where we have put $c_j \equiv \frac{1}{2} e^{i\varphi_1} F_1 c^{(j)}$. The combination of Eq. (A7) with the relations (A2) produces Eqs. (24).

One can take advantage of the special form of the matrix A in (A4) to simplify the calculation of the eigenvalues. Because the first pulse is ultrashort and thus energetically broader, it may be assumed that $N_1 > N_2$. Then the formula

$$\begin{aligned} \det \begin{bmatrix} D^{(1)} - E & \frac{1}{2}\Lambda \\ \frac{1}{2}\tilde{\Lambda} & D^{(2)} - E \end{bmatrix} \\ = \det \left[(D^{(2)} - E) - \frac{1}{4} \tilde{\Lambda} (D^{(1)} - E)^{-1} \Lambda \right] \det[(D^{(1)} - E)] \end{aligned} \quad (\text{A8})$$

produces a simpler determinant. For $N_2 = 1$ (A8) gives

$$\begin{aligned} \left[(E_j - z_{N_1+1} + E_g + \omega_1 + \omega_2) - \sum_{i=1}^{N_1} \frac{\frac{1}{4} \Lambda_{iN_1+1}^2}{E_j - z_i + E_g + \omega_1} \right] \\ \times \prod_{k=1}^{N_1} (E_j - z_k + E_g + \omega_1) = 0, \end{aligned} \quad (\text{A9})$$

where $j = 1, \dots, N_1 + 1$ and the eigenvalues are determined from the factor in the square brackets. This is a well-known form that describes a set of states in the presence of a perturber, which, in our case, is the localized part of the second channel.

For the simple case $N_1 = N_2 = 1$, treated in Ref. [18], Eq. (A9) gives

$$E_{1,2} = (z_1 - E_g - \omega_1) + (a \pm \lambda)/2, \quad (\text{A10})$$

where $a = z_2 - z_1 - \omega_2$ is the complex detuning and $\lambda = \sqrt{a^2 + \Lambda_{11}^2}$ is the Rabi frequency.

APPENDIX B

In the case where the envelope function is a Gaussian, i.e., $g_1(t) = e^{-\frac{(t-t_0)^2}{2\sigma_a^2}}$, the integrals $G(E, t)$ of Eq. (29a) are expressed in terms of the *error function* defined as

$$\int_0^t dt' e^{-c^2 t'^2} = \frac{\sqrt{\pi}}{2c} \operatorname{erf}(ct). \quad (\text{B1})$$

From the basic integral (B1) one easily obtains

$$G(\varepsilon, t_0, t) \equiv \int_{t_0}^t dt' e^{-c^2(t'-t_0)^2 + i\varepsilon t'} = \frac{\sqrt{\pi}}{2c} e^{-\frac{\varepsilon^2}{4c^2} + i\varepsilon t_0} \{\operatorname{erf}[c(t - t_0 + t_\varepsilon)] - \operatorname{erf}[c(t_0 - t_0 + t_\varepsilon)]\}, \quad (\text{B2})$$

where

$$t_\varepsilon = -i\varepsilon/2c^2. \quad (\text{B3})$$

In the above formulas, $c = \frac{1}{\sigma_a\sqrt{2}}$. Consequently, $\operatorname{Re}t_\varepsilon = \sigma_a^2 \operatorname{Im}\varepsilon$, and the real part of the time t_ε , although expected to be generally small, can have a significant value in the case of a broad Gaussian.

-
- [1] F. Krausz and M. Ivanov, Attosecond physics, *Rev. Mod. Phys.* **81**, 163 (2009).
- [2] T. Schultz and M. Vrakking (eds.), *Attosecond and XUV Physics* (Wiley-VCH, Weinheim, Germany, 2014).
- [3] F. Calegari, G. Sansone, S. Stagira, C. Vozzi, and M. Nisoli, Advances in attosecond science, *J. Phys. B: At. Mol. Opt. Phys.* **49**, 062001 (2016).
- [4] M. Hentschel, R. Kienberger, Ch. Spielmann, G. A. Reider, N. Milošević, T. Brabec, P. Corkum, U. Heinzmann, M. Drescher, and F. Krausz, Attosecond metrology, *Nature (London)* **414**, 509 (2001).
- [5] P. M. Paul, E. S. Toma, P. Breger, G. Mullot, F. Augi, Ph. Balcou, H. G. Muller, and P. Agostini, Observation of a train of attosecond pulses from high harmonic generation, *Science* **292**, 1689 (2001).
- [6] C. A. Nicolaides, Th. Mercouris, and Y. Komninos, Attosecond dynamics of electron correlation in doubly excited states, *J. Phys. B: At. Mol. Opt. Phys.* **35**, L271 (2002).
- [7] M. Schultze, M. Fieß, N. Karpowicz, J. Gagnon, M. Korbman, M. Hofstetter, S. Neppl, A. L. Cavalieri, Y. Komninos, Th. Mercouris *et al.*, Delay in photoemission, *Science* **328**, 1658 (2010). See, also, the supporting online material.
- [8] E. Goulielmakis, Z.-H. Loh, A. Wirth, R. Santra, N. Rohringer, V. S. Yakovlev, S. Zherebtsov, T. Pfeifer, A. M. Azzeer, M. F. King *et al.*, Real-time observation of valence electron motion, *Nature (London)* **466**, 739 (2010).
- [9] R. Pazourek, S. Nagele, and J. Burgdörfer, Attosecond chronoscopy of photoemission, *Rev. Mod. Phys.* **87**, 765 (2015).
- [10] M. Isinger, R. J. Squibb, D. Busto, S. Zhong, A. Harth, D. Kroon, S. Nandi, C. L. Arnold, M. Miranda, J. M. Dahlström *et al.*, Photoionization in the time and frequency domain, *Science* **358**, 893 (2017).
- [11] A. Kaldun, A. Blättermann, V. Stooß, S. Donsa, H. Wei, R. Pazourek, S. Nagele, C. Ott, C. D. Lin, J. Burgdörfer, and T. Pfeifer, Observing the ultrafast buildup of a Fano resonance in the time domain, *Science* **354**, 738 (2016).
- [12] Th. Mercouris, Y. Komninos, and C. A. Nicolaides, Time-dependent formation of the profile of the He $2s2p^1P^o$ state excited by a short laser pulse, *Phys. Rev. A* **75**, 013407 (2007); **87**, 069905(E) (2013).
- [13] C. A. Nicolaides, Attosecond-resolved electron dynamics in many-electron atoms: Quantitative theory and comparison with measurements, *Appl. Sci.* **8**, 533 (2018).
- [14] J. J. Omiste and L. B. Madsen, Attosecond photoionization dynamics in neon, *Phys. Rev. A* **97**, 013422 (2018).
- [15] C. Ott, L. Aufleger, T. Ding, M. Rebholz, A. Magunia, M. Hartmann, V. Stooß, D. Wachs, P. Birk, G. D. Borisova *et al.*, Strong-Field Extreme-Ultraviolet Dressing of Atomic Double Excitation, *Phys. Rev. Lett.* **123**, 163201 (2019).
- [16] C. A. Nicolaides, Theoretical approach to the calculation of energies and widths of resonant (autoionizing) states in many-electron atoms, *Phys. Rev. A* **6**, 2078 (1972).
- [17] Y. Komninos, Th. Mercouris, and C. A. Nicolaides, Theory and computation of electromagnetic transition matrix elements in the continuous spectrum of atoms, *Eur. Phys. J. D* **71**, 8 (2017).
- [18] Y. Komninos, Th. Mercouris, and C. A. Nicolaides, Discrete-resonance-resonance transitions, induced by two pulses with ultrashort time delay: Formal analytic solution and quantitative applications, *Phys. Rev. A* **98**, 023428 (2018).
- [19] S. L. Cousin, N. di Palo, B. Buades, S. M. Teichmann, M. Reduzzi, M. Devetta, A. Kheifets, G. Sansone and J. Biegert, Attosecond Streaking in the Water Window: A New Regime of Attosecond Pulse Characterization, *Phys. Rev. X* **7**, 041030 (2017); X. Ren, J. Li, Y. Yin, K. Zhao, A. Chew, Y. Wang, S. Hu, Y. Cheng, E. Cunningham, Y. Wu *et al.*, Attosecond light sources in the water window, *J. Optics* **20**, 023001 (2018).
- [20] J. Li, X. Ren, Y. Yin, K. Zhao, A. Chew, Y. Cheng, E. Cunningham, Y. Wang, S. Hu, Y. Wu *et al.*, 53-attosecond X-ray pulses reach the carbon K-edge, *Nat. Commun.* **8**, 186 (2017).
- [21] Y. Pertot, C. Schmidt, M. Matthews, A. Chauvet, M. Huppert, V. Svoboda, A. von Conta, A. Tehlar, D. Baykusheva, J.-P. Wolf, and H. J. Wörner, Time-resolved x-ray absorption spectroscopy

- with a water window high-harmonic source, *Science* **355**, 264 (2017).
- [22] M. Tronc, G. C. King, and F. H. Read, Carbon K-shell excitation in small molecules by high-resolution electron impact, *J. Phys. B: At. Mol. Phys.* **12**, 137 (1979).
- [23] D. R. Beck and C. A. Nicolaides, Inner electron binding energies and Auger energies in free atoms for use in X-ray spectroscopy, *J. Elect. Spect. Rel. Phenom.* **8**, 249 (1976).
- [24] P. Bisgaard, R. Bruch, P. Dahl, B. Fastrup, and M. Rødbro, Measurement of free-atom K-shell binding energies of light elements, *Phys. Scripta* **17**, 49 (1978).
- [25] D. R. Beck and C. A. Nicolaides, Theory of one-electron binding energies including correlation, relativistic and radiative effects: Application to free atoms and metals, in *Excited States in Quantum Chemistry*, edited by C. A. Nicolaides and D. R. Beck (Reidel, Dordrecht, Holland, 1979), p. 329.
- [26] C. A. Nicolaides, Y. Komninos, and D. R. Beck, K-shell binding energy of Be and its fluorescence yield, *Phys. Rev. A* **27**, 3044 (1983).
- [27] D. R. Beck and C. A. Nicolaides, Theory of Auger energies in free atoms: Application to the alkaline earths, *Phys. Rev. A* **33**, 3885 (1986).
- [28] U. Fano, Effects of configuration interaction on intensities and phase shifts, *Phys. Rev.* **124**, 1866 (1961).
- [29] C. A. Nicolaides, Th. Mercouris, and Y. Komninos, Time-dependent formation of the profile of resonance atomic states and its dependence on the duration of ultrashort pulses from free-electron lasers, *Phys. Rev. A* **80**, 055402 (2009).